Table of Contents

Appendix Figure S1

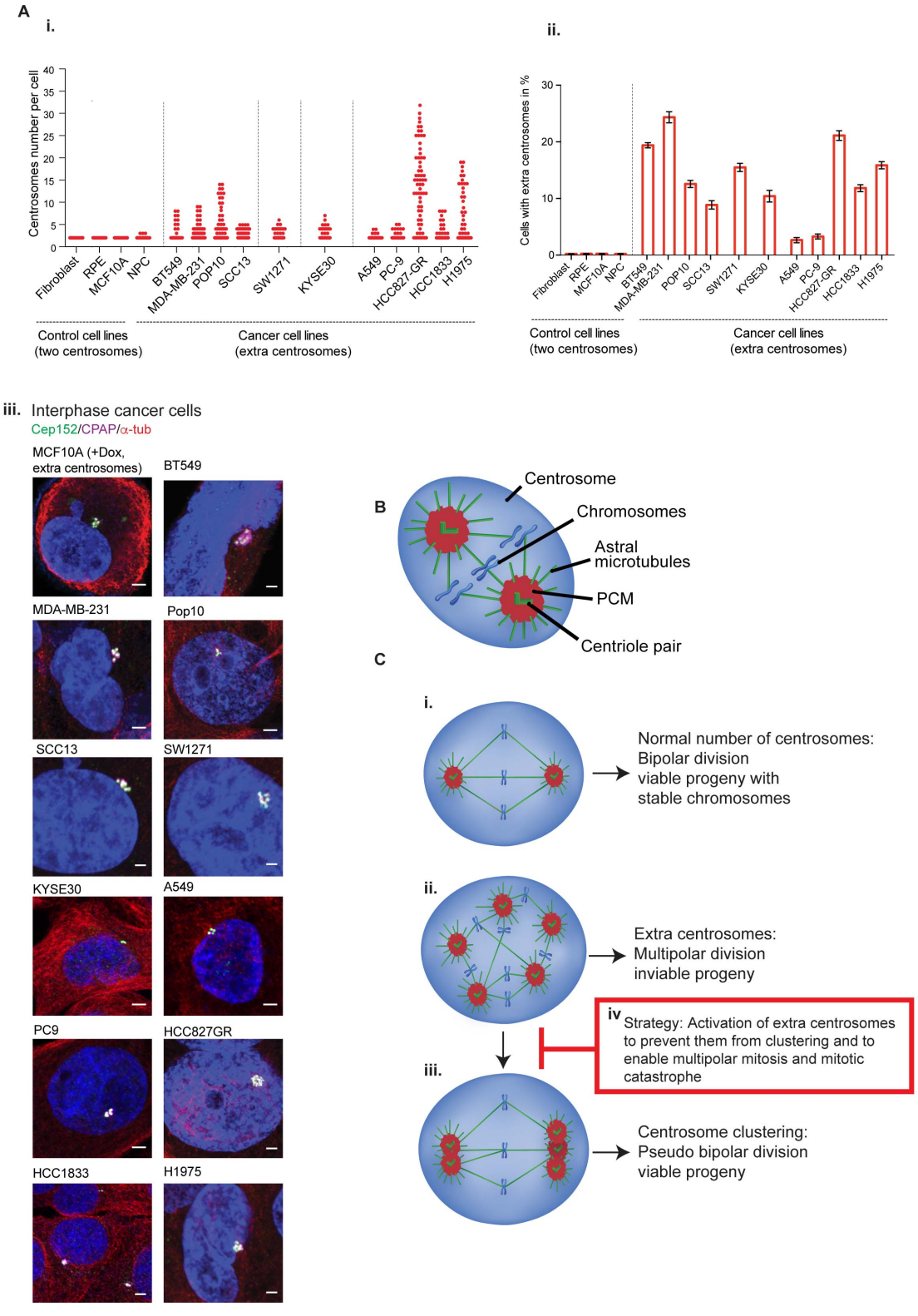

Appendix Figure S1: Cancer cells exhibit extra centrosomes.

(A) Analysis of centrosome numbers in various normal (Retinal Pigment Epithelial cells, Fibroblasts, MCF10A and Neural progenitor cells) and cancer cell types **(i)**. An extreme increase in centrosome numbers is found in TKI (Tyrosine Kinase Inhibitor)-resistant NSCLC (non-small cell lung cancer) cell lines carrying somatic and activating mutations in EGFR ($PC9^{EGFR\text{-}Exon19del}$,

H1975^{T790M}, HCC827-GR with MET-amplification) (Ahsan, 2016; Engelman et al, 2007; Guo et al, 2008; Pagliarini et al, 2015). Other cancer cell lines that exhibit extra centrosomes include BT549, MDA-MB-231 (triple negative breast cancer), Pop10, SCC13, SW1271$^{p53/pRb/CDKN2Adel}$, KYSE30$^{p53/MYC/CyclinD1}$ and KRAS mutant A549^{G12S} NSCLC. Superscripts represent mutations, deletions or abnormalities in the respective genes. Note that many cells display an overlapping centrosome numbers. Bar graph on right shows the percentage of cells with extra centrosomes. At least 500 cells in each cancer cell types were considered. **(ii)** Breast cancer cell line MDA-MB-231 and lung cancer cell line HCC827-GR showed higher percentages of extra centrosome compared to other cancer cell lines and primary cell lines. Data represent mean ± SEM of three independent experiments (*N*)=*3,* (*n*=400-600 cells). **(iii)** Clustered interphase extra centrosomes exhibit reduced or no microtubule nucleation. MCF10A (+Dox, extra centrosomes, these MCF10A cells are engineered to overexpress Polo-like-kinase-4 (Plk4) to induce centrosome amplification upon doxycycline induction(Godinho et al, 2014)) and other cancer cells harboring extra centrosomes remained inactive with reduced microtubule-nucleation at interphase. All these cells were stained with Cep152 (green), CPAP (magenta), microtubules (α-tubulin, red) and DNA (DAPI blue). Scale bar, 2μm.

(B) Schematic overview. A cartoon shows a normal metaphase cell with a pair of centrosomes. Centriolar pair (green), peri-centriolar material (PCM, red) and microtubules (green) are shown. Centrosomes are matured at this stage as they recruit an enhanced level of PCM and nucleate robust microtubules.

(C) Normal cells containing two centrosomes undergo bipolar mitosis **(i)**. Cancer cells harboring extra centrosomes can form multipolar spindles and these cells can undergo multipolar mitosis leading to non-viable progeny **(ii)**. However, cancer cells with extra centrosomes could cluster their extra centrosomes to form a pseudobipolar spindle **(iii)**. This process is named as “centrosome clustering” (Ganem et al, 2009; Kramer et al, 2002; Leber et al, 2010). Thus, via extra centrosome clustering, cancer cells generate pseudo-bipolar spindles to circumvent deleterious effects of centrosomal amplification caused by mitotic catastrophe. Preventing extra centrosomes from clustering is a strategy to enable them to undergo mitotic catastrophe and selective cell death (Red box) **(iv)**.

Appendix Figure S2

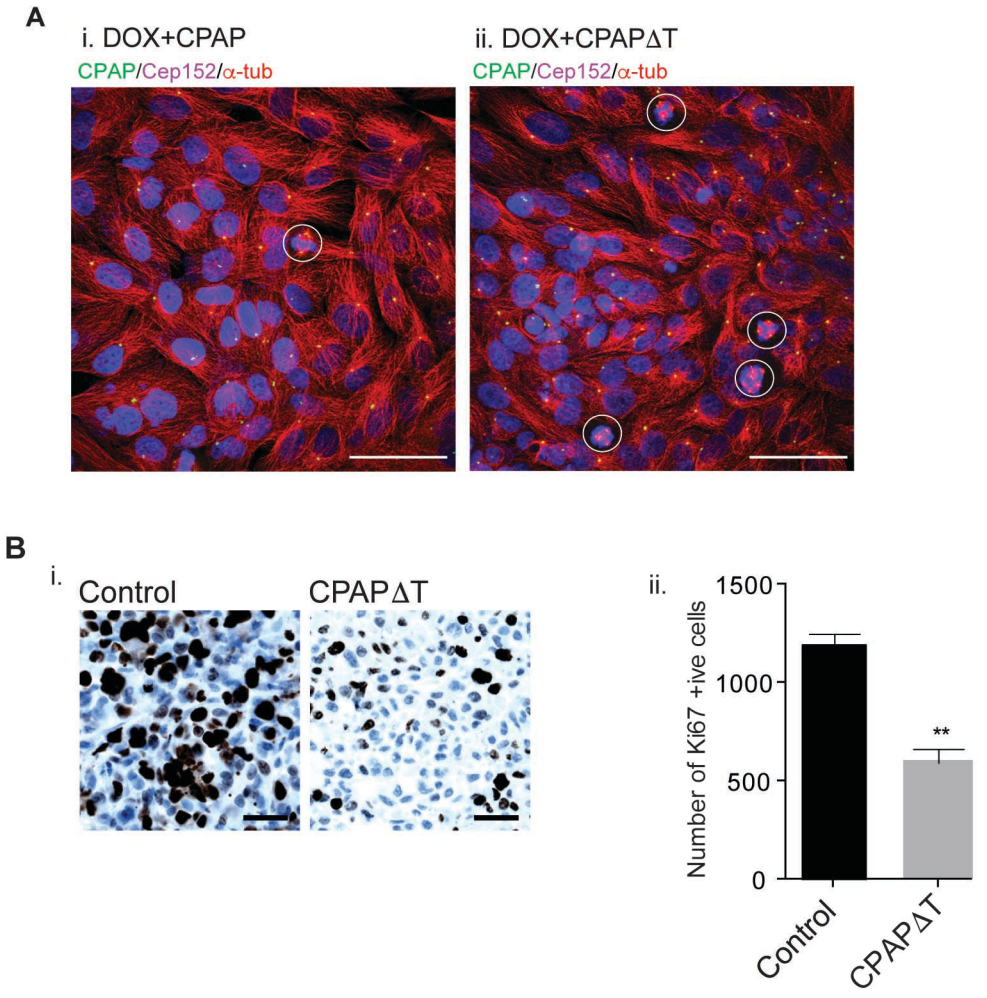

Appendix Figure S2, related to Fig 1: Genetic perturbation of CPAP-Tubulin interaction prevents clustering of extra centrosomes.

(A) Overview of immunofluorescent images of MCF10A cells overexpressing CPAP-WT and CPAPΔT (a mutant version of CPAP that does not bind to tubulin). These MCF10A cells are engineered to overexpress Polo-like-kinase-4 (Plk4) to induce centrosome amplification upon doxycycline induction (Dox+)(Godinho et al, 2014). Cells expressing CPAP-WT show clustered extra centrosomes in mitosis (circled, left panel). Expressing CPAPΔT prevents extra centrosomes from clustering and causes multipolar mitosis (circled, right panel). Cells were induced with doxycycline (2μg/ml) for 48 hours and stained with Cep152 (green), microtubules (α-tubulin, red) and DNA (DPAI, blue). Scale bar, 20μm.

(B) Cell proliferation is reduced in CPAPΔT but not in CPAP-WT expressing MDA-MB-231 xenograft tumors as indicated by Ki67 staining **(i).** Bar graph shows number of Ki67-positive cells between CPAP-WT (control) and CPAPΔT expressing MDA-MB-231 xenograft tumors **(ii).** Data

are obtained from three different tumors and represented as mean ± SEM. Unpaired *t*-test. ***P* < 0.001. Scale bar, 20μm.

Appendix Figure S3

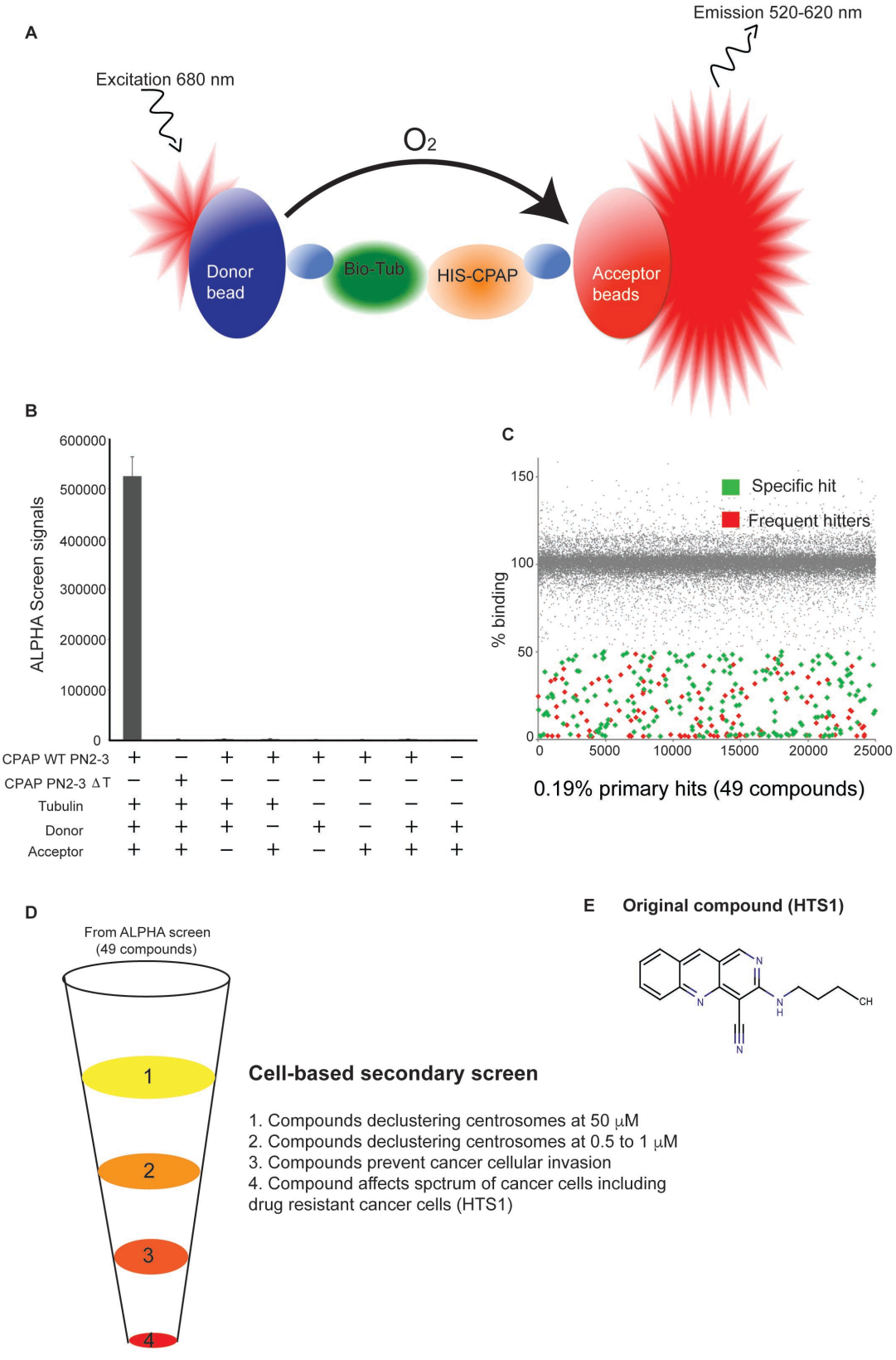

Appendix Figure S3: AlphaScreen assay to identify CPAP-Tubulin inhibitors.

(A) Design of an AlphaScreen assay for high-throughput screening (HTS) to identify CPAP-tubulin inhibitors. The chemiluminescence assay relies on a Streptavidin donor bead that recognizes the

biotinylated tubulin and a Nickel-NTA acceptor bead that binds to His-tagged CPAP protein. The conserved PN2-3 domain of CPAP that harbors a tubulin-binding region is used(Clement et al, 2008; Hsu et al, 2008; Zheng et al, 2016). Interaction of CPAP-tubulin brings both beads in close proximity to generate luminescence. In the presence of CPAP-tubulin inhibitor reduced emission is observed at 520-620 nm.

(B) The CPAP-tubulin protein interaction produced robust AlphaScreen signals with an overall Z prime of Z'=0.84 and signal window of SW=19.34. The first bar in the graph represents wild type protein pairs. The second bar represents reduced signal coming from CPAP mutant (CPAP mutant CPAPΔT that does not interact with tubulin)-tubulin interaction. The conserved PN2-3 domain (amino acid 319-389) of CPAP that harbors its tubulin-binding region is used(Clement et al, 2008; Gopalakrishnan et al, 2012; Hsu et al, 2008; Zheng et al, 2016). Moreover, various combinations lacking either of the proteins or beads are displayed. The graph indicates a representative experiment with three technical replicates. In total, AlphaScreen experiment with wild type and mutant protein was carried out at least five times.

(C) Scatter plots of HTS. The CPAP-tubulin protein interaction was screened against a library of 25,000 compounds (Diverse set of drug-like compounds obtained from 10,000 ChemDiv; 10,000 Enamine; 5,000 Chembridge). Inactive compounds are marked in grey. Specific hits and frequent hitters are marked in green and red, respectively. The screening yielded excellent screening parameter: Z' = 0.84; %CVmax = 5.09; SW = 19.34 (all values mean of n = 80).

(D) Schematic representation of cell-based secondary screen and hit selection. The primary hits (49 compounds) were screened and selected based on their ability to activate centrosomes and to prevent cancer cell proliferation (monolayer and spheroids).

(E) HTS1, the parent compound obtained from the secondary screen.

Appendix Figure S4

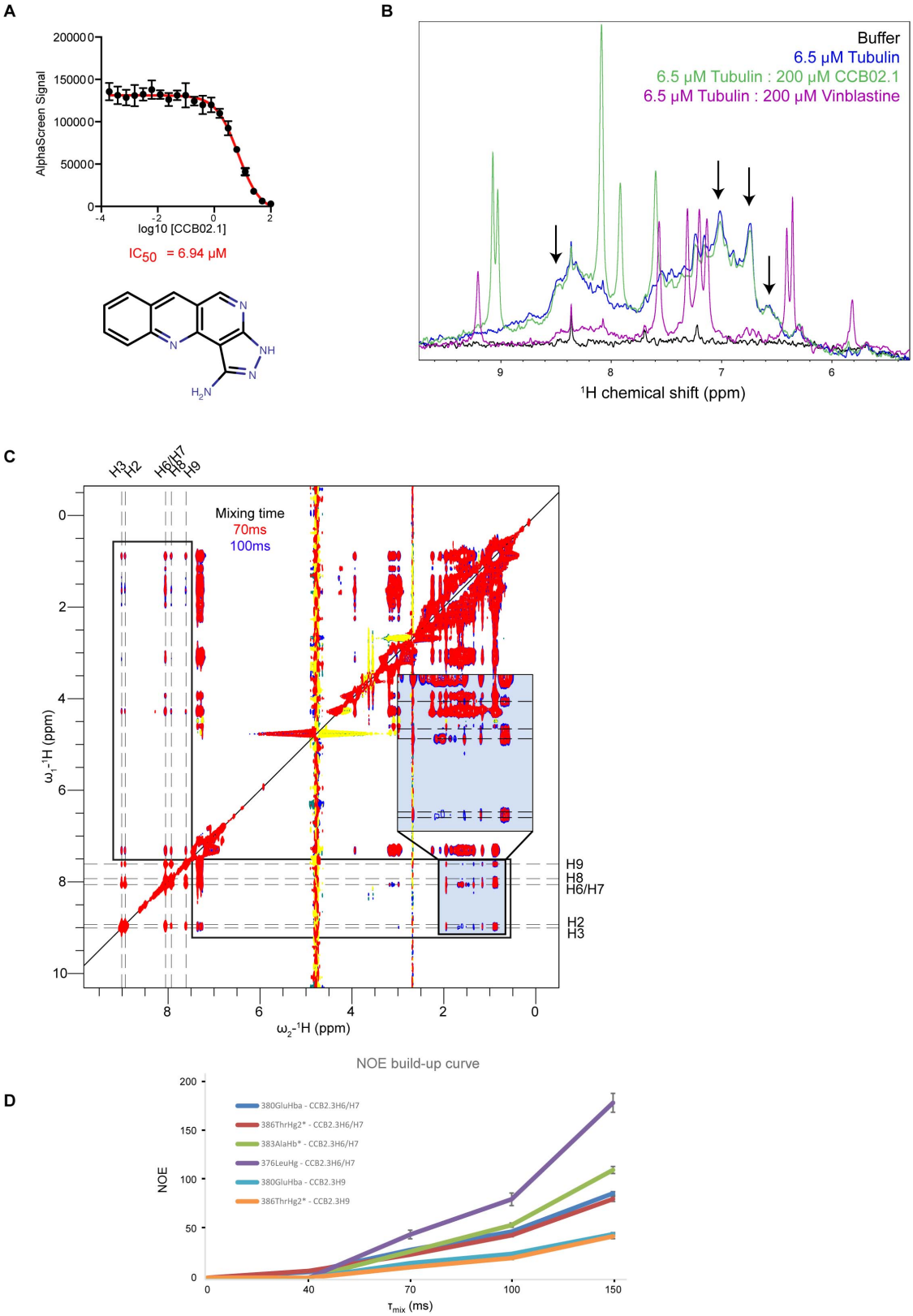

Appendix Figure S4, related to Fig 2: CCB02 is a tubulin binder.

(A) CCB02.1, the optimized derivative of CCB02 exhibits a dose-dependent reduction of CPAP-tubulin AlphaScreen signal. Error bars indicate data from a triplicate determination.

(B) To make sure that tubulin at 6.5μM used in the NMR analysis is folded properly and not forming aggregation, we performed ^{1}H-1D NMR spectra of tubulin in its free form (blue), in complex with CCB02.1 (green) and Vinblastine (purple) and compared each other. No significant changes in tubulin are observed when it is in complex with CCB02.1 while the signal intensity of tubulin decreases substantially in the presence of Vinblastine**.** It is known that Vinblastine binds at the interface between tubulin heterodimers(Gigant et al, 2005). In this case, the signal intensity of tubulin in the ^{1}H -1D NMR experiment would decrease (as observed in our experiments). If tubulin had polymerized, the interface between heterodimers would not be accessible for Vinblastine binding. These experiments indicate that our experimental conditions do not influence tubulin to undergo polymerization or aggregation.

(C) NMR experiments were performed to map the tubulin-binding site and to derive structural information for CCB02-tubulin interaction. For this purpose, a twelve-amino acid peptide (residues 375-386 of CPAP) was used, which is a part of the conserved loop-helix motif of CPAP's PN2-3 region that mediates microtubule binding to the outer surface on β-tubulin. To enhance interligand NOEs using the INPHARMA approach comparable binding affinities of the CPAP peptide and compound to tubulin are required. A longer version of CPAP peptide (residues 372-394) has an affinity of ~4μM , therefore, we used compound CCB02.1, a derivative of CCB02 that prevents the CPAP-tubulin interaction with IC_{50}=6.94μM. Two-dimensional NOESY NMR spectra were recorded for a mixture of CPAP peptide (400μM), CCB02.1 (200μM) and tubulin (6.5μM) at different mixing times (40, 70, 100, 150ms). NOESY spectra at 70ms and 100ms mixing times are shown in red and blue, respectively. Boxes highlight regions of the spectra where inter-ligand NOEs (INPHARMA peaks) are observed. The strongest intermolecular NOE peaks appeared between H6/H7 hydrogen atoms of CCB02.1 and Phe375/385Hε* hydrogen atoms of the CPAP peptide. As the Hε* signals of CPAP Phe375 and Phe385 have very similar chemical shifts an unambiguous analysis of the INPHARMA NOEs was not possible. We thus focused on the weaker but well-resolved correlations with the Hδ* protons. The Phe385 Hδ* correlations exhibit more intense peaks to H6/H7 of CCB02.1 suggesting that CCB02.1 has a preference for binding to the Phe385 pocket in β-tubulin. In the control experiments, no intermolecular NOEs were observed when CPAP peptide and CCB02.1 were mixed in 1:1 ratio in the absence of tubulin (data not shown).

(D) NOE build-up curve of six well-resolved intermolecular NOE peaks show a damped-parabolic shape, characteristic of inter-ligand NOE cross peaks arising from protein-mediated spin diffusion (INPHARMA). This indicates that the CPAP peptide and CCB02.1 bind to an overlapping binding

site on the tubulin surface. The NOE peak intensities are normalized to the diagonal peak intensity of the proton in ω_2 and multiplied by 10^4 as described by Reese et al., 2007(Reese et al, 2007).

Appendix Figure S5

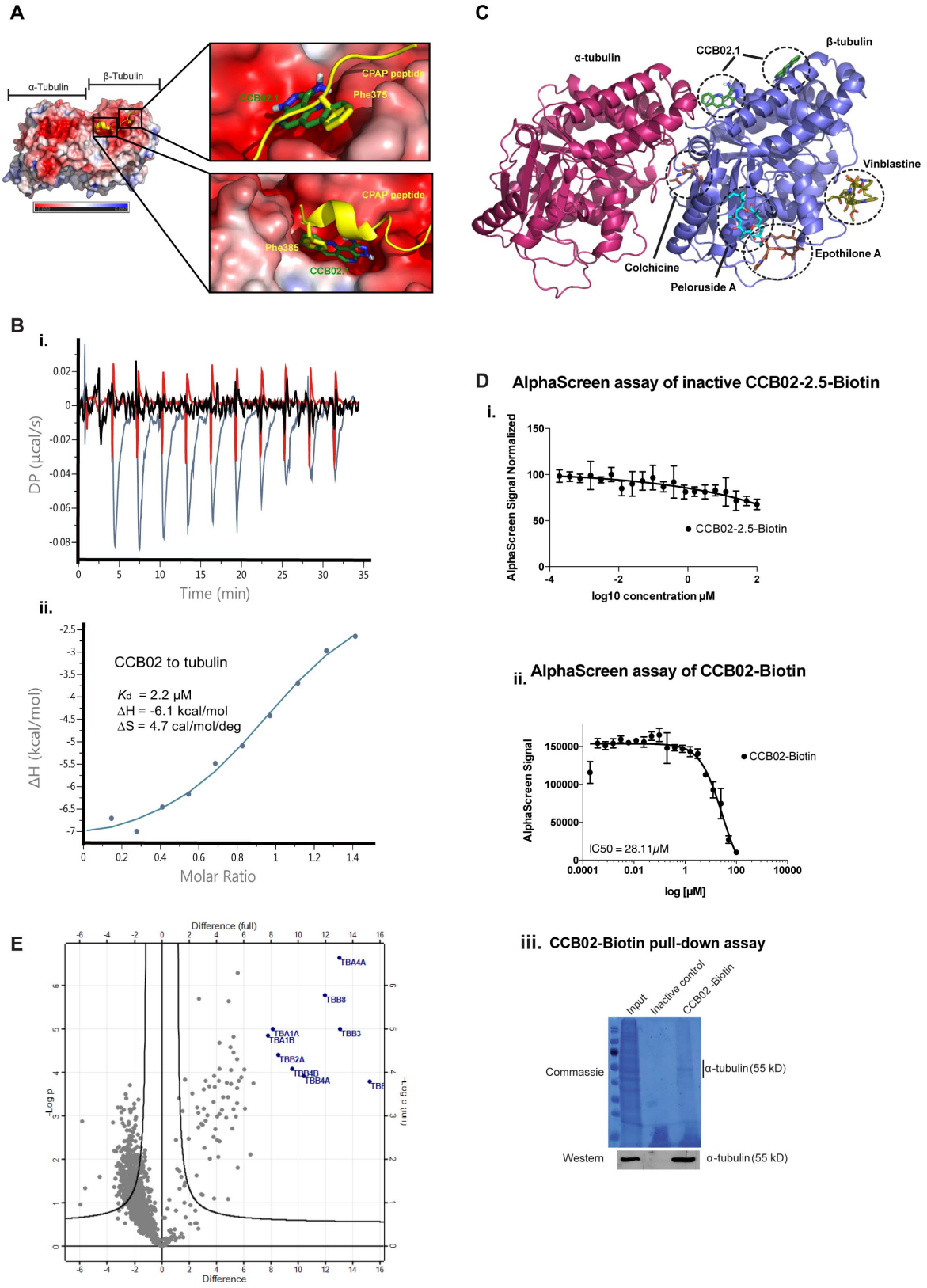

Appendix Figure S5, related to Fig 2 and Fig 7: CCB02 is a tubulin binder but does not appear to occupy the binding sites of conventional tubulin binders.

(A) *In silico* docking of CCB02.1 with tubulin using the CPAP peptide-binding site as the grid box, suggests that CCB02.1 can occupy both the CPAP Phe385 and Phe375 binding pockets on tubulin but with a preference for the Phe385 pocket (in 8 out of 10 docking models generated, CCB02.1 is found in the Phe385 pocket)**.** Crystal structure of the CPAP-tubulin complex with the CPAP peptide shown in yellow and tubulin shown as surface colored by electrostatic surface potential. Zoomed view for the binding pockets for CPAP Phe375 and Phe385. Upper and lower panels show the binding poses of CCB02.1 (green) relative to CPAP peptide (yellow). The models agree with our NMR experiments where we observed the most intense inter ligand NOE peaks of CCB02.1 H6/H7 to F375/385Hε* but weaker signals to other protons throughout the peptide **(Fig. 2B).** These data suggest that CCB02.1 has a preference for the Phe385 pocket. In any case the NMR data and the *in-silico* modeling demonstrate that CCB02 is a novel tubulin binder, with a binding site that overlaps with the hydrophobic pockets that recognize conserved phenylalanine residues of at the outer surface of β-tubulin. This binding mode indicates that CCB02 can compete and perturb the CPAP-tubulin interaction.

(B) (i) ITC titration curves. Black, buffer to tubulin titration control; Red, CCB02 to buffer titration control; Light blue, CCB02 to tubulin titration. Calorimetric experiments were conducted at 15 °C with a MicroCal PEAQ-ITC instrument (Malvern). Tubulin samples were dialyzed against the 1×BRB80 buffer (80mM PIPES-K, 1mM MgCl2, 1mM EGTA, pH 6.8, 0.5% DMSO) prior to titration. And the lyophilized compound CCB02 was solubilized using the dialysis buffer. For all ITC titration curves, 25μM tubulin and 173μM compound CCB02 were used. Protein concentration was determined by absorbance spectroscopy at 280nm. Compound was quantified by weighing on a large scale. **(ii)** ITC titration fitting curve. Acquired calorimetric titration data were analyzed using MicroCal PEAQ-ITC Analysis Software using the One Set of Binding Sites fitting model.

(C) Binding locations of known tubulin binders. The binding sites of known inhibitors and the docking model with CCB02.1 with tubulin are indicated on the structure of the tubulin. PDB accession codes 1Z2B (Vinblastine), 4O4J (Peloruside A), 4O4I (Epothilone A), 4O2B (Colchicine).

(D) While Biotinylated CCB02 **(**CCB02-Biotin) exhibits a dose-dependent reduction of CPAP-tubulin AlphaScreen signal **(i)**, biotinylated inactive CCB02 analog **(**CCB02-2.5-Biotin) does not perturb CPAP-tubulin interaction **(ii)**. Error bars indicate data from a triplicate determination. **(iii)** Coomassie and Western blot of CCB02-biotin binding to tubulin from cellular extracts. Control pull down used CCB02-2.5-biotin, an inactive analog of CCB02 (Inactive control).

(E) Volcano plot representing proteins of label-free pull-down of CCB02. The logarithmic ratio of protein LFQ intensities in CCB02/lysate pull-downs (x-axis; difference) were plotted against

negative logarithmic p-values (y-axis; -log p) of the t-test performed from triplicates. A hyperbolic curve separates significant CCB02-interacting proteins. All the significant tubulin isoforms are marked (in blue).

Appendix Figure S6

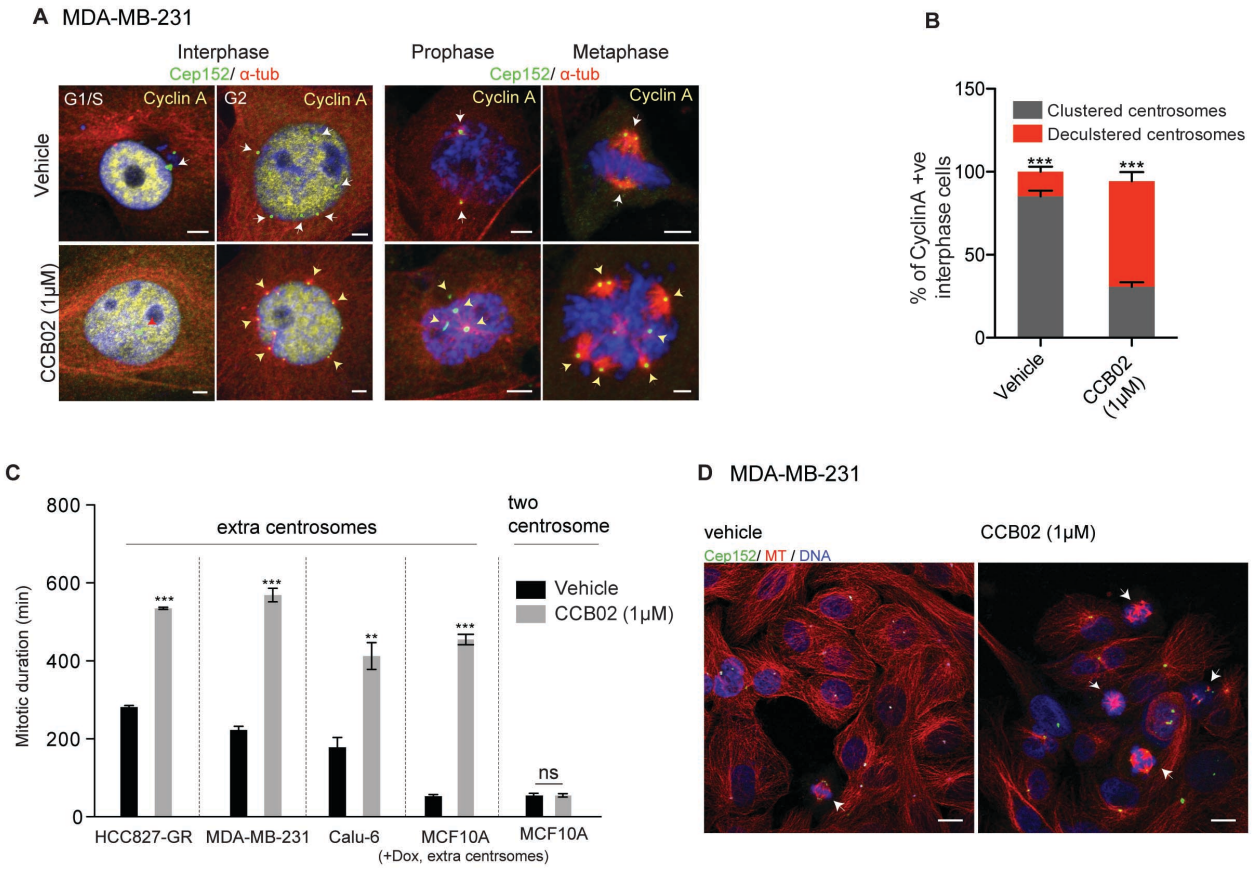

Appendix Figure S6, related to Fig 3: CCB02 activates centrosomes prior to mitosis and prolongs the mitotic duration.

(A) CCB02 activates extra centrosomes before the onset of mitosis. Interphase MDA-MB-231 cells treated with CCB02 or vehicle are marked by Cyclin A staining (yellow), a bona-fide G1-S transition marker(Hochegger et al, 2008). In vehicle-treated groups, Cyclin A-positive cells exhibit extra centrosomes with less or no microtubule nucleation (white arrows). Note, CCB02-treated cells exhibit declustered extra centrosomes each nucleating enhanced levels of microtubule asters (red and yellow arrows).

Panels at right: Prophase and metaphase cells are not positive for Cyclin A. Cells are stained for Cyclin A (yellow), Cep152 (green), microtubules (α-tubulin, red) and DNA (DAPI, blue). Scale bar, 2μm.

(B) Bar diagram profiles percentages of Cyclin A-positive interphase cells exhibiting declustered centrosomes each nucleating microtubules. Data represent mean ± SEM of three independent

experiments, (*N*)=*3,* (*n*=200 cells per condition). *p* values were obtained using Two-way ANOVA test.***$P < 0.0001$.

(C) Bar graph represents the mitotic duration of vehicle and CCB02 (1μM) treated cancer cells in minutes. Cells with higher percentage of centrosome amplification such as, MDA-MB-231 and HCC827 GR spend more time in mitosis compared to other cancer cells. Data represent mean ± SEM of three independent experiments (*N*)=*3,* (*n*=70 cells per condition). *p* values were obtained using unpaired t test.**$P < 0.001$, ***$P < 0.0001$.

(D) Fixed images of vehicle and CCB02-treated MDA-MB-231 cells. CCB02-treated cells show an obvious increase in number of mitotic cells compared to vehicle-treated cultures (arrows). This indicates that upon CCB02 treatment cancer cells harboring extra centrosomes have a tendency to undergo a prolonged mitosis. Cells are stained with Cep152 (green), MT (tubulin, red) and DNA (DAPI, blue). Scale bar, 10μm.

Appendix Figure S7

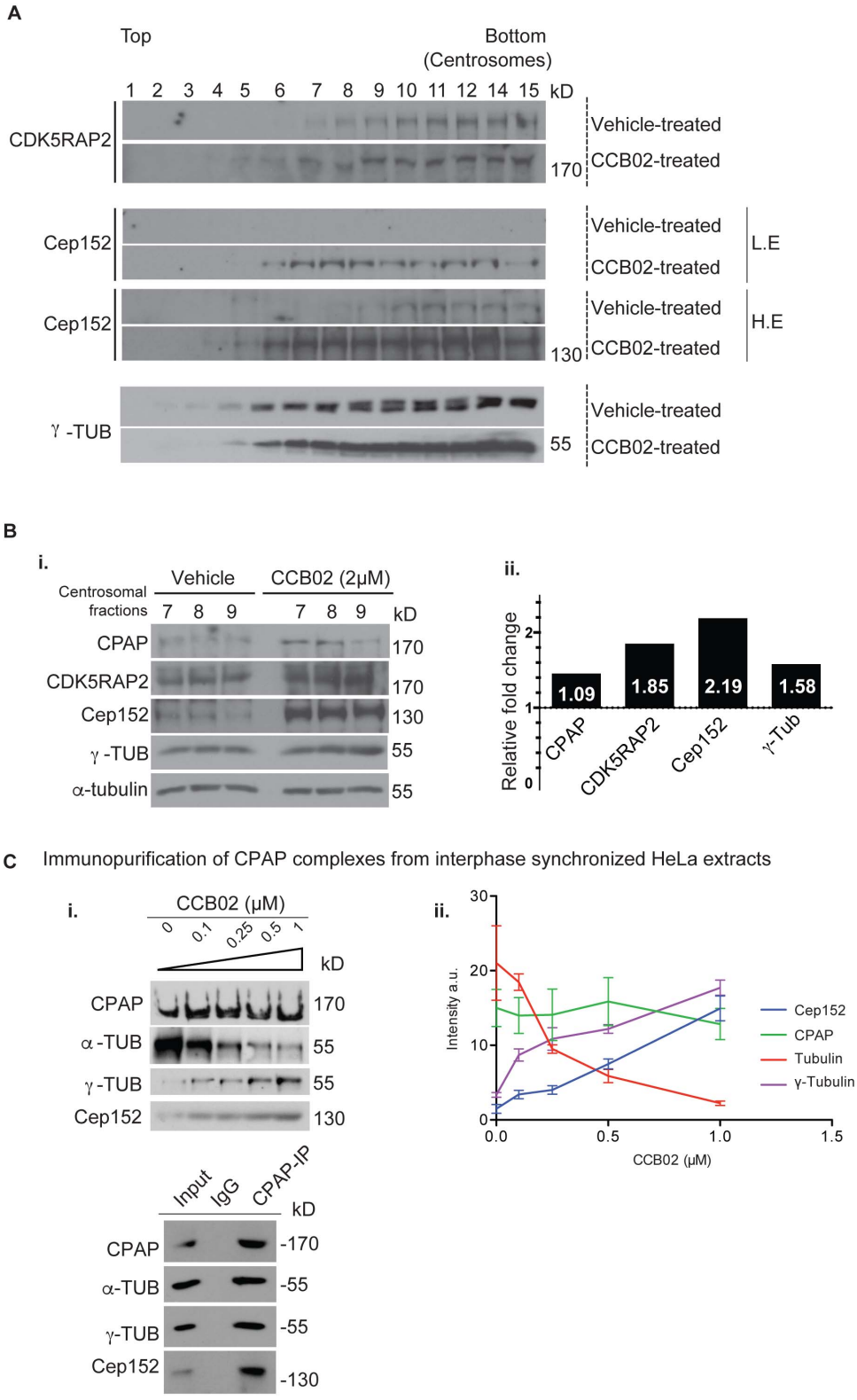

Appendix Figure S7, related to Fig 5: CCB02 prevents CPAP-tubulin interaction in cells and causes CPAP to bind an enhanced amount of its binding partners.

(A) Western blot analysis of complete fractions of vehicle or CCB02 treated cellular extracts isolated using sucrose gradient velocity sedimentation. A discontinuous gradient was prepared manually using 35, 50 and 75% of sucrose. After ultracentrifugation, centrosomes are fractionated at bottom. CCB02-treated centrosomes contain an increased amount of PCM proteins (Cep152, CDK5RAP2 and γ-tubulin) as compared to vehicle-treated cells. For Cep152, both low- and high-exposure blots are shown. Cells were treated with CCB02 at a concentration of 2μM for 48 hours.

(B) Sucrose gradient fractionation of centrosomes isolated from vehicle or 2μM of CCB02-treated MCF10A cells. Centrosomes fractioned from CCB02-treated MCF10A cell extracts show increased levels of CDK5RAP2, Cep152 and γ-tubulin **(i)** Only centrosomal fractions sedimented at the bottom of the sucrose gradient is blotted **(ii)** Bar graph indicate relative fold change of CPAP-interacting proteins in comparison to vehicle treated control.

(C) Immunopurification of CPAP complexes purified from interphase-synchronized HeLa cell extracts in the presence and absence of CCB02 **(i)** increasing concentrations of CCB02 progressively prevents tubulin binding to CPAP allowing CPAP to bind an enhanced amount of Cep152 and γ-tubulin. Control IP experiment is shown below. **(ii)** Plot showing PCM protein intensities co-immunoprecipitated with CPAP at various concentrations of CCB02 treatment. Data represent mean ± SEM. (*N*)=3.

Appendix Figure S8

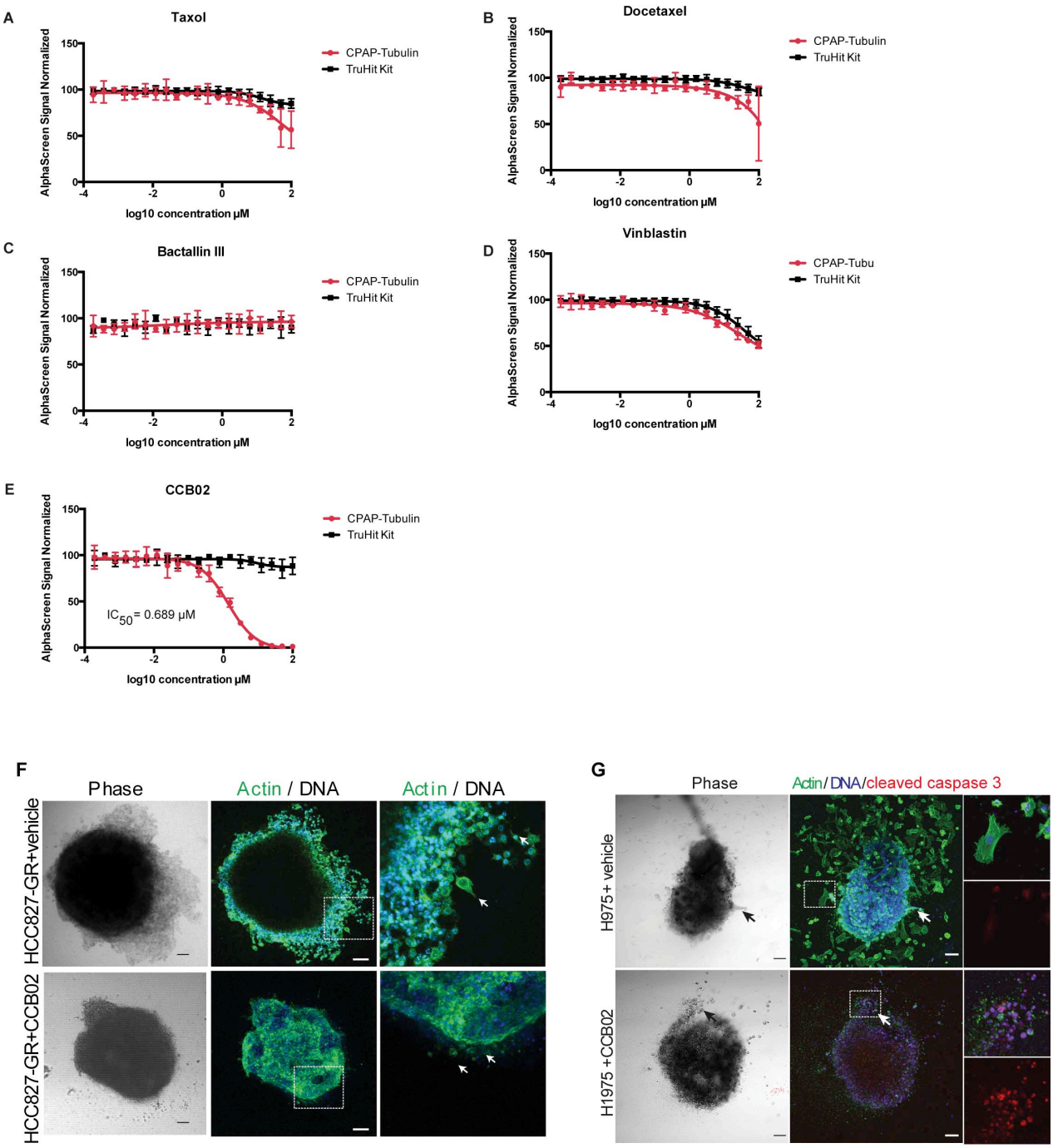

Appendix Figure S8, related to Fig 7 and Movie-EV3A-C: CCB02 but not conventional tubulin binders inhibit CPAP-Tubulin interaction.

Normalized AlphaScreen signal for conventional tubulin binders, Paclitaxel **(A)**, Docetaxel **(B)**, Bactallin III **(C)**, Vinblastine **(D)** compared to CCB02 **(E)**. CCB02 exhibited a dose-dependent reduction of CPAP-tubulin interaction, whereas the conventional tubulin binders did not show any reduction in the signal. This indicates that CPAP-tubulin interaction is specific for CCB02. Error

bars indicate data from a triplicate determination. The TruHit Kit captures possible effects on AlphaScreen assay technology**.**

(F) Real time live imaging of HCC827-GR (MET-amplification) with vehicle or 5μM CCB02. At the end of live imaging, spheroids were fixed and stained for F-actin (green) and DNA (blue). Arrow indicates invasive (vehicle-treated) and non-invasive (CCB02-treated) structures in spheroids. Scale bar, 100μm.

(G) Anti-invasive activity of CCB02 in organotypic cultures. $H1975^{T790M}$ spheroids were treated with vehicle or 5μM CCB02. After 48 hours, spheroids were fixed and stained for F-actin (green), activated caspase-3 (red) and DNA (blue). CCB02 treated spheroids exhibit rounded cells characteristics of prolonged mitotic arrest (arrows). These rounded cells exhibit and increased cleaved caspase-3 activity suggestive of apoptosis. On the other hand, vehicle-treated spheroids display actin-positive invasive protrusions emerging from $H1975^{T790M}$ spheroids (arrows) Scale bar, 100μm.

REFERENCES

Ahsan A (2016) Mechanisms of Resistance to EGFR Tyrosine Kinase Inhibitors and Therapeutic Approaches: An Update. *Adv Exp Med Biol* **893:** 137-153

Clement MJ, Savarin P, Coutant J, Toma F, Curmi P (2008) NMR assignment of PN2-3, a tubulin interaction subdomain of the CPAP protein. *Biomol NMR Assign* **2:** 115-117

Engelman JA, Zejnullahu K, Mitsudomi T, Song Y, Hyland C, Park JO, Lindeman N, Gale CM, Zhao X, Christensen J, Kosaka T, Holmes AJ, Rogers AM, Cappuzzo F, Mok T, Lee C, Johnson BE, Cantley LC, Janne PA (2007) MET amplification leads to gefitinib resistance in lung cancer by activating ERBB3 signaling. *Science* **316:** 1039-1043

Ganem NJ, Godinho SA, Pellman D (2009) A mechanism linking extra centrosomes to chromosomal instability. *Nature* **460:** 278-282

Gigant B, Wang C, Ravelli RB, Roussi F, Steinmetz MO, Curmi PA, Sobel A, Knossow M (2005) Structural basis for the regulation of tubulin by vinblastine. *Nature* **435:** 519-522

Godinho SA, Picone R, Burute M, Dagher R, Su Y, Leung CT, Polyak K, Brugge JS, Thery M, Pellman D (2014) Oncogene-like induction of cellular invasion from centrosome amplification. *Nature* **510:** 167-171

Gopalakrishnan J, Frederick Chim YC, Ha A, Basiri ML, Lerit DA, Rusan NM, Avidor-Reiss T (2012) Tubulin nucleotide status controls Sas-4-dependent pericentriolar material recruitment. *Nature cell biology* **14:** 865-873

Guo A, Villen J, Kornhauser J, Lee KA, Stokes MP, Rikova K, Possemato A, Nardone J, Innocenti G, Wetzel R, Wang Y, MacNeill J, Mitchell J, Gygi SP, Rush J, Polakiewicz RD, Comb MJ (2008) Signaling networks assembled by oncogenic EGFR and c-Met. *Proceedings of the National Academy of Sciences of the United States of America* **105:** 692-697

Hochegger H, Takeda S, Hunt T (2008) Cyclin-dependent kinases and cell-cycle transitions: does one fit all? *Nature reviews Molecular cell biology* **9:** 910-916

Hsu WB, Hung LY, Tang CJ, Su CL, Chang Y, Tang TK (2008) Functional characterization of the microtubule-binding and -destabilizing domains of CPAP and d-SAS-4. *Exp Cell Res* **314:** 2591-2602

Kramer A, Neben K, Ho AD (2002) Centrosome replication, genomic instability and cancer. *Leukemia* **16:** 767-775

Leber B, Maier B, Fuchs F, Chi J, Riffel P, Anderhub S, Wagner L, Ho AD, Salisbury JL, Boutros M, Kramer A (2010) Proteins required for centrosome clustering in cancer cells. *Science translational medicine* **2:** 33ra38

Pagliarini R, Shao W, Sellers WR (2015) Oncogene addiction: pathways of therapeutic response, resistance, and road maps toward a cure. *EMBO Rep* **16:** 280-296

Reese M, Sanchez-Pedregal VM, Kubicek K, Meiler J, Blommers MJ, Griesinger C, Carlomagno T (2007) Structural basis of the activity of the microtubule-stabilizing agent epothilone a studied by NMR spectroscopy in solution. *Angewandte Chemie* **46:** 1864-1868

Zheng X, Ramani A, Soni K, Gottardo M, Zheng S, Ming Gooi L, Li W, Feng S, Mariappan A, Wason A, Widlund P, Pozniakovsky A, Poser I, Deng H, Ou G, Riparbelli M, Giuliano C, Hyman AA, Sattler M, Gopalakrishnan J, Li H (2016) Molecular basis for CPAP-tubulin interaction in controlling centriolar and ciliary length. *Nature communications* **7:** 11874